Forebrain-Specific B-Raf Deficiency Reduces NMDA Current and Enhances Small-Conductance Ca2+-Activated K+ (SK) Current

Cornelia Ruxanda , Christian Alzheimer , Fang Zheng *

Posted Date: 26 June 2025

doi: 10.20944/preprints202506.2192.v1

Keywords: B-raf; synaptic transmission; NMDA current; small-conductance Ca2+-activated K+ (SK) channels; hippocampus

 doi:10.20944/preprints202506.2192.v1

Article

Forebrain-Specific B-raf Deficiency Reduces NMDA Current and Enhances Small-Conductance Ca^{2+}-Activated K^+ (SK) Current

Cornelia Ruxanda, Christian Alzheimer and Fang Zheng *

Institute of Physiology and Pathophysiology, Friedrich-Alexander-Universität Erlangen-Nürnberg, 91054 Erlangen, Germany

* Correspondence: fang.zheng@fau.de; Tel.: +49-9131-8529300

Abstract

B-raf is a crucial player within the ERK/MAPK signaling pathway. In the CNS, B-raf has been implicated in neuronal differentiation, long-term memory and major depression. Mice with forebrain neuron-specific B-raf knockout show behavioral deficits in spatial learning tasks and impaired hippocampal long-term potentiation (LTP). To elucidate the mechanism(s) underlying diminished synaptic plasticity in B-raf-deficient mice, we performed whole-cell recordings from CA1 pyramidal cells in hippocampal slices of control and B-raf mutant mice. We found that the NMDA/AMPA ratio of excitatory postsynaptic currents (EPSCs) at the Schaffer collateral – CA1 pyramidal cell synapses was significantly reduced in B-raf mutants, which would at least partially account for their impaired LTP. Interestingly, the reduced NMDA-component of field postsynaptic potentials in mutant preparations was partially reinstated by blocking the apamin-sensitive small-conductance Ca^{2+}-activated K^+ (SK) channels, which have also been reported to modulate hippocampal LTP and learning tasks. To determine the impact of B-raf-dependent signaling on SK current, we isolated the apamin-sensitive tail current after a strong depolarizing event and found indeed a significantly bigger SK current in B-raf-deficient cells compared to controls, which is consistent with the reduced action potential firing and the stronger facilitating effect of apamin on CA1 somatic excitability in B-raf-mutant hippocampus. Our data suggest that B-raf signaling readjusts the delicate balance between NMDA receptors and SK channels to promote synaptic plasticity and facilitate hippocampal learning and memory.

Keywords: B-raf; synaptic transmission; NMDA current; small-conductance Ca^{2+}-activated K^+ (SK) channels; hippocampus

1. Introduction

Raf (rapidly accelerated fibrosarcoma) proteins with serine/threonine kinase activity distribute widely in tissues including the brain. As effectors for Ras and Rap1 and activators for MEK/ERK, raf proteins stand in a linear kinase cascade of ERK/MAPK signaling pathway, regulating cell proliferation and survival, development, and cognition [1-5]. Among the three raf isoforms (A-, B- and C-raf), B-raf is a stronger activator for ERK/MAPK signaling pathway, with higher MEK binding affinity [6, 7]. As mutations in various B-raf domains are associated with human diseases including mental disorders and tumors, B-Raf is a prime target for molecule-based therapies [8-11]. In the brain, B-raf is widely distributed in the neuronal soma and the neuritic processes, with its highest immunoreactivity in the hippocampus [12, 13]. Using lentivirus-based rapid gene replacement method in cultured rodent slices and human ESC-induced and iPSC-derived neurons, Lim et al. found that large-scale disease-linked loss- or gain-of-function B-raf mutations induced a wide range of changes in synaptic transmission, closely correlated with the extent of cognitive deficits [14]. With

 doi:10.20944/preprints202506.2192.v1

this big data analysis, the authors identified B-raf as the universal signaling effector relaying canonical NMDAR-CaMKII-SynGap-Ras signaling to the MEK-ERK cascade at synapses [14].

Animal studies showed that global B-raf deletion was embryonically lethal [15], and conditional knockout of B-raf in the forebrain glutamatergic neurons from the second postnatal week affected anxiety/depression-like behavior, and impaired hippocampal-dependent spatial learning [16, 17]. Such conditional B-raf deletion compromised ERK phosphorylation and reduced the magnitude of long-term potentiation (LTP) at the glutamatergic synapses formed by Schaffer collaterals (SC) onto CA1 pyramidal cells [16]. LTP is usually induced by brief high frequency tetanic stimulation, which produces a strong temporal summation of excitatory postsynaptic potentials and depolarization in postsynaptic cells. This causes the relief of the Mg^{2+} block of NMDA receptor (NMDA-R), leading to a strong calcium influx which activates intracellular signaling cascades including CaMKII and ERK/MAPK pathway and ultimately potentiates AMPA receptor (AMPA-R) mediated synaptic transmission [18, 19].

Notably, transient elevations of intracellular Ca^{2+} following NMDA-R activation, Ca^{2+} influx via voltage-dependent Ca^{2+} channels during depolarization, as well as calcium release from intracellular Ca^{2+} stores, also activate small-conductance Ca^{2+}-activated potassium channels (SK channels) [20-23]. SK channels distribute widely along dendrites and soma [24, 25]. Especially, SK channels localize strategically to the postsynaptic density of dendritic spines where they form a Ca^{2+}-mediated negative feedback loop with synaptic NMDA-Rs [26-28], thus fine-tuning the NMDA-R-dependent synaptic plasticity and learning [29-31]. By combining whole-cell patch-clamp recordings and extracellular field potential recordings in mouse brain slice preparation, we identified reduced NMDA current and enhanced SK current in B-raf mutant pyramidal cells as complementary mechanisms for cognitive impairments.

2. Results

Mice with conditional B-raf deletion showed reduced LTP in the hippocampal CA1 region [16]. Because LTP of the SC-CA1 synapses is NMDA-R dependent, we first examined whether the NMDA component of excitatory transmission is affected by B-raf deficiency. Using whole-cell voltage-clamp recordings, we pharmacologically isolated the CNQX-sensitive AMPA-EPSC (excitatory postsynaptic current; Vh set to -80 mV) and the APV-sensitive NMDA-EPSC (Vh set to +40 mV). As shown in Figure 1, the NMDA/AMPA ratio, calculated by dividing the peak amplitude of NMDA-EPSC by that of AMPA-EPSC, was indeed significantly reduced in B-raf mutant py-ramidal cells (control, 34.56 ± 3.40 %, n = 7 form 5 mice; B-raf$^{-/-}$, 25.67 ± 2.22 %, n = 9 from 5 mice; p = 0.039). Such reduction in NMDA/AMPA ratio at SC-CA1 synapses would at least partially account for their impaired LTP.

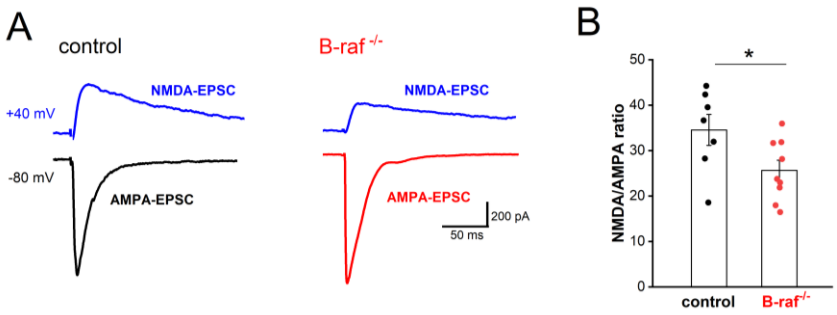

Figure 1. Reduced NMDA/AMPA ratio in B-raf-deficient hippocampus. Whole-cell voltage-clamp recordings were performed in hippocampal CA1 pyramidal cells, in the presence of $GABA_A$ receptor antagonist picrotoxin (100 μM), to measure NMDA and AMPA components of excitatory postsynaptic currents (EPSCs) at SC - CA1

 doi:10.20944/preprints202506.2192.v1

pyramidal cell synapses. (**A**) Membrane potential of recorded cells was clamped either at -80 mV to monitor AMPA receptor-mediated EPSCs (AMPA-EPSCs) or at +40 mV for NMDA receptor-mediated EPSCs (NMDA-EPSCs), as depicted by current traces from a control (*left*) and a B-raf$^{-/-}$ (*right*) slice. (**B**) Summary of NMDA/AMPA ratio, calculated by dividing the peak amplitude of respective EPSCs in individual cells. Statistical comparison was performed using unpaired, two-tailed student's t-test. * $p < 0.05$.

Among the different mechanisms mitigating the NMDA response, one intriguing candidate is the immediate negative feedback regulation of NMDA currents due to the close spatial coupling between NMDA receptors and SK channels in dendritic spines of CA1 pyramidal cells [26]. This well-established concept holds that calcium influx through NMDA receptors activates SK channels, which in turn short-circuit NMDA currents and promote their Mg^{2+} block. To determine whether B-raf-dependent signaling has an impact on SK channel activity in the dendrites, we examined the effect of the selective SK channel blocker apamin on CA1 synaptic transmission in control and B-raf-deficient hippocampi, by monitoring field postsynaptic potentials (fPSPs) in CA1 stratum radiatum. Consistent with a previous report [16, but see 14], basic synaptic transmission at the SC-CA1 synapse was not changed in B-raf$^{-/-}$ slices, as demonstrated by the nearly perfect superposition of the input-output (I-O) curves that depicts peak fPSPs amplitude as function of stimulus strength for both genotypes (Figure 2A). Given the well-known Mg^{2+} block of NMDA-Rs at resting potentials, CA1 fPSP responses to single SC stimulation should be predominantly mediated by AMPA receptors. In fact, application of the AMPA-R blocker CNQX (20 μM) strongly suppressed fPSPs (Figure 2A, *inset*); even high stimulus intensity (up to 400 μA) failed to produce sizable NMDA responses (Figure 2A). It was only when we used a brief burst-like stimulation paradigm consisting of 3 stimuli @ 100 Hz, which mimics natural firing patterns of hippocampal pyramidal cells during information processing [32], that we elicited a significant CNQX-insensitive fPSP component that was carried by NMDA-Rs as it was abrogated by the NMDA-R antagonist APV (50 μM; Figure 2B, *inset*). Unlike the AMPA component, the NMDA component of the fPSP was significantly reduced in slices of B-raf$^{-/-}$ mice when compared to their control counterparts (Figure 2B), with maximal responses (to stimulus intensity 400 μA) of 2.11 ± 0.14 mV in controls (n = 7 form 4 mice) and 1.53 ± 0.09 mV in mutants (n = 10 form 5 mice; p = 0.003).

Next, we examined the impact of the SK channel inhibitor, apamin (125 nM, 30 min) on the NMDA component in control and mutant slices (Figure 2C). Comparison of the I-O curves before and during apamin superfusion showed a significant increase in NMDA-fPSPs for both genotypes (Figures 2D-E). When we normalized the apamin-induced increase of the NMDA component to the respective pre-drug values, we made the interesting finding that the effect of apamin in slices from transgenic mice was lower for weak stimuli (80 μA) but higher for strong stimuli (400 μA), when compared to control slices (Figure 2F). As a consequence of the latter, apamin equalized the difference in maximal NMDA-fPSPs between genotypes (at stimulus intensity 400 μA: control in apamin, 2.54 ± 0.19 mV, n = 5; B-raf$^{-/-}$ in apamin, 2.64 ± 0.28 mV, n = 6; p = 0.780) (Figures 2D-E).

Considering the widespread distribution of SK channels along dendrites and somata of CA1 pyramidal cells, we wondered whether B-raf deficiency would also alter their effect on somatic excitability. For this purpose, we performed field potential and whole-cell recordings in the CA1 pyramidal cell layer to examine population response (termed as population spike, PS) and individual cellular firing of action potentials (APs), respectively. In extracellular PS recordings from the cell body layer, electrical stimulation of SC in stratum radiatum produced a positive-going voltage trajectory reflecting EPSP in the apical dendrites. While still rising, the positive-going trajectory was interrupted by a sharp negative deflection, which is the extracellular correlate of somatic APs once the EPSP became suprathreshold, and the PS was completed with a second positive-going trajectory representing putative feedback inhibition (Figure 3A, *inset)*. Plots of averaged peak PS amplitude against increasing stimulus intensity did not reveal appreciable differences between genotypes (Figure 3A). When the stimulus intensity was adjusted to evoke 30-40 % of maximal response, application of apamin (125 nM) after stable baseline led to a gradual increase in PS amplitude, which

 doi:10.20944/preprints202506.2192.v1

reached steady-state after 25 min (Figure 3B). Resembling the behavior of the NMDA component in the mutant preparation at maximal stimulus intensity (Figure 2F), PS responses in B-raf-deficient slices displayed higher sensitivity to the SK channel blocker than controls (26-30 min in apamin: control, 118.50 ± 5.23 % of baseline value, n = 8 from 4 mice; B-raf$^{-/-}$, 139.57 ± 8.45 % of baseline value, n = 7 from 5 mice; p = 0.048).

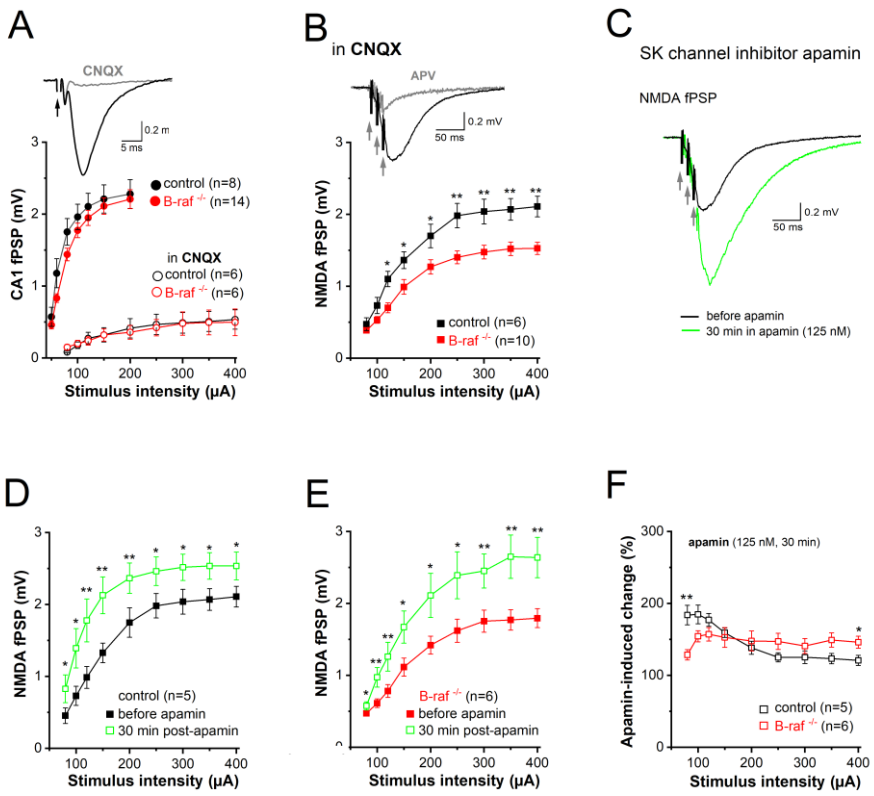

Figure 2. Decreased NMDA receptor-mediated synaptic transmission in CA1 pyramidal cells of B-raf-deficient mice. Field postsynaptic potentials (fPSP) were monitored extracellularly in CA1 stratum radiatum, in response to electric stimulation of SC by single stimulus (**A**) or by a burst of 3 stimuli (at 100 Hz; **B-F**). (A) Input-output (I-O) curves from control and B-raf mutant slices, in the absence and in the presence of AMPA receptor antagonist CNQX (20 µM). Traces on top are recordings from a control slice, illustrating typical field potentials before and during CNQX application (stimulus strength at 80 µA). Arrow indicates truncated stimulus artifact. (**B**) I-O curves for burst stimulus-induced NMDA-fPSPs in the presence of CNQX. Inset depicts suppression of NMDA-fPSP by APV (50 µM). (**C**) Apamin facilitates NMDA-fPSP (stimulus strength 80 µA). (**D-E**) I-O curves for apamin-enhanced NMDA-fPSPs in control (**D**) and B-raf-deficient slices (**E**), which were normalized in (**F**) to reveal relative augmenting effect of apamin as function of stimulus intensity for the two genotypes. Statistical comparisons were performed using ANOVA followed by Tukey's post-hoc test. * $p < 0.05$; ** $p < 0.01$.

In whole-cell current-clamp recordings, CA1 pyramidal cells from controls and B-raf mutants had comparable resting membrane potentials (control, -65.80 ± 1.90 mV, n = 10 from 4 mice; B-raf$^{-/-}$, -67.20 ± 2.78 mV, n = 6 from 4 mice; p = 0.680), and membrane input resistances (measured at -70 mV: control, 177.50 ± 13.79 MΩ; B-raf$^{-/-}$, 183.16 ± 16.41 MΩ; p = 0.556). APs were evoked by depolarizing steps (50, 100 and 200 pA) for 500 ms (Figure 3C, inset), with membrane potential pre-set to -70 mV by current injection. As summarized in Figure 3C, B-raf mutant cells fired significantly less APs upon small suprathreshold depolarization (50 pA; control, 4.89 ± 0.61 APs per pulse; B-raf$^{-/-}$, 2.20 ± 0.73 APs per pulse; p = 0.019), but for stronger depolarizations, the firing frequency vs. depolarizing current relationship (f-I curve) for the two groups appeared to converge gradually (Figure 3C). Further kinetic analysis of individual APs did not reveal alterations in AP amplitude and half-with (Figures

 doi:10.20944/preprints202506.2192.v1

3D-E), nor in voltage threshold (control, -58.05 ± 0.80 mV; B-raf$^{-/-}$, -56.79 ± 1.14 mV; p = 0.383) or in maximal rising slope (control, 292.98 ± 18.73 mV/ms; B-raf$^{-/-}$, 316.18 ± 18.24 mV/ms; p = 0.352). However, a strong increase in medium afterhy-perpolarization (mAHP), measured 30-50 ms after AP repolarization, was evident in mutant cells (control, 4.53 ± 0.25 mV; B-raf$^{-/-}$, -8.13 ± 0.99 mV; p = 0.0005; Figure 3E).

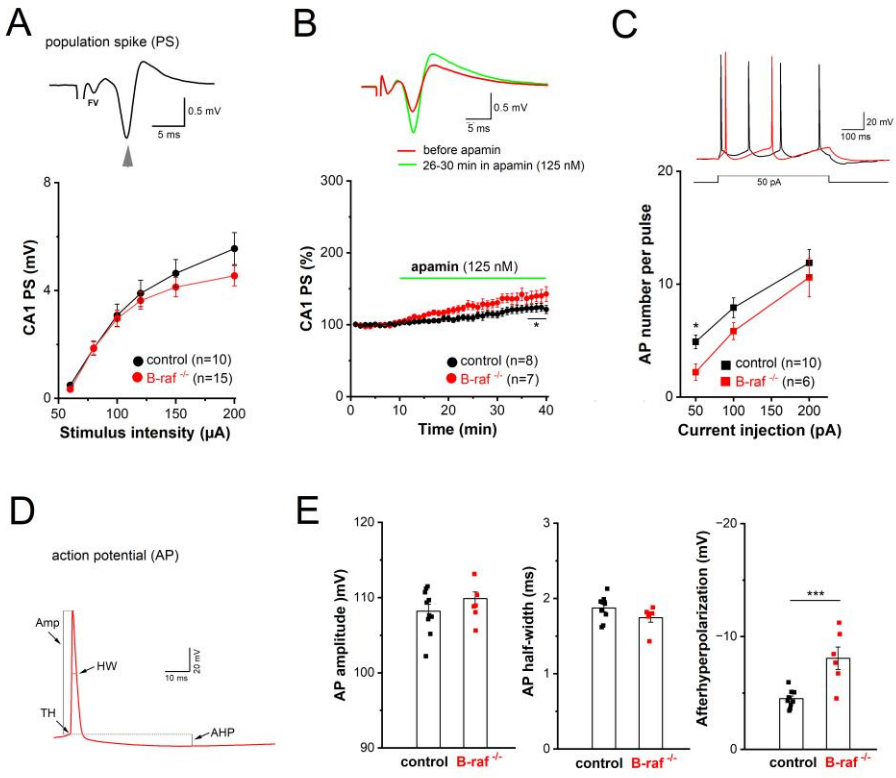

Figure 3. Reduced somatic excitability of CA1 pyramidal cells in B-raf-deficient mice. (**A-B**) Population spikes (PS) were recorded in CA1 pyramidal cell layer, in response to electric stimulation of SC. (**A**) I-O curves of PS amplitude vs. stimulus intensity in control and B-raf$^{-/-}$ slices. Inset depicts stimulus-induced waveform in control slice. Arrowhead points towards negative peak of PS, stimulus artifact is truncated. FV, fiber volley. (**B**) Comparison of time course of PS augmentation during apamin application between genotypes. Inset depicts averaged PS from B-raf-mutant slice before and 26-30 min after onset of apamin administration (stimulus intensity 80 µA). (**C**) Action potentials (APs) of control and B-raf$^{-/-}$ CA1 pyramidal cells, recorded in whole-cell current-clamp mode. AP firing was elicited by depolarizing current steps 500 ms long from membrane potential pre-set to -70 mV, as exemplified by superimposed traces from a control (black trace) and a B-raf-deficient cell (red trace). Plots below depict relationship between firing rate and size of depolarizing current for the two groups. (**D**) Waveform of first AP after onset of depolarizing current injection (50 pA) in B-raf$^{-/-}$ cells, illustrating the parameters analyzed and summarized in histograms of (**E**). TH threshold, Amp Amplitude, HW half-width. Statistical comparisons were performed using one-way ANOVA followed by Tukey's post-hoc test (**A-C**) or unpaired, two-tailed student's t-test (**E**). * $p < 0.05$; *** $p < 0.001$.

Our findings that, firstly, B-raf deficiency renders PS responses more sensitive to apamin, and that, secondly, the f-I curve in the mutant preparation is attenuated compared to the control condition, might be most parsimoniously explained in terms of an upregulation of SK currents across dendritic and somatic compartments. To substantiate this hypothesis, we performed whole-cell voltage-clamp recordings from CA1 pyramidal cells (Vh -60 mV), using an established protocol to directly examine the currents involved in mAHP generation. In this paradigm, neurons are de-

 doi:10.20944/preprints202506.2192.v1

polarized to +30 mV for 100 ms, which produces a "tail current" upon returning to -60 mV (Figure 4A). TTX (1 μM) and TEA (5 mM) were used to block Na^+ channels and other K^+ channels (such as A-type K^+ channels, BK channels), respectively. To isolate their SK-mediated component, we measured "tail currents" in the absence and presence of apamin (125 nM, 20-30 min, Figure 4A). Upon subtraction of the currents, the peak amplitude of the SK-dependent tail current was 136.89 ± 9.88 pA in B-raf$^{-/-}$ cells (n = 9 from 4 mice), which was significantly larger than in control cells (91.60 ± 7.24 pA, n = 10 from 5 mice; p = 0.002; Figure 4B).

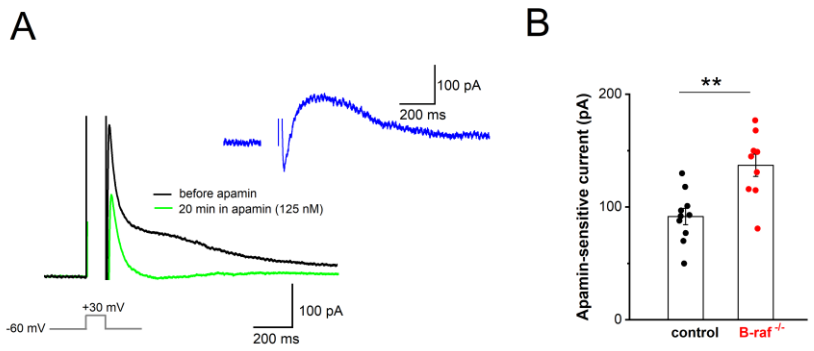

Figure 4. Enhanced contribution of SK current to mAHP in B-raf-deficient mice. (**A**) "Tail current" responses after step depolarization to +30 mV for 100 ms in the absence and presence of apamin (Vh -60 mV; in 1 μM TTX and 5 mM TEA) which, after subtraction, yielded pure apamin-sensitive current (*inset,* blue trace). (**B**) Histogram summarizes apamin-sensitive currents in control and B-raf$^{-/-}$ cells. Statistical comparison was performed using unpaired, two-tailed student's t-test. ** $p < 0.01$.

3. Discussion

In the present study, we demonstrate that CA1 pyramidal cells in brain slices from B-raf-deficient mice exhibit reduced NMDA currents and stronger SK currents, when compared to their counterparts in slices from control mice. The close proximity of NMDA receptors and SK channels at the postsynaptic site enables a local negative feed-back mechanism to contain NMDA responses, as the activation of NMDA receptors triggers the subsequent opening of Ca^{2+}-activated SK channels [26, 27]. In the absence of B-raf signaling, the inverse changes of NMDA and SK currents would operate in concert to impair NMDA-R dependent LTP at SC-CA1 pyramidal cell synapses, thereby offering a plausible explanation for the poor performance of B-raf-deficient mice in hippocampus-dependent learning and memory tasks [16]. In addition, we found that SK currents are also enhanced in the somatic region of CA1 pyramidal cells, where, by strengthening mAHPs, they serve to control firing rate. We thus propose that the enhancement of SK current in B-raf-deficient mice has a dual impact on signal processing in CA1 pyramidal cells, affecting both their input (feed-back inhibition of NMDA currents) and their output (reduced firing rate due to augmented mAHP).

In the soma and proximal dendrites of hippocampal pyramidal cells, SK channels are activated by Ca^{2+} influx resulting mainly from AP-induced opening of L-type Ca^{2+} channels [33, 34]. AP-linked Ca^{2+} transients are maximal in the soma and the proximal apical dendrites and decrease rapidly with distance from the soma [34]. The resultant outflow of K^+ during SK activation contributes, together with the M-current, to the generation of an AHPs of medium duration (mAHP) following AP discharge [33, 35-38]. In addition to showing a significantly enhanced mAHP in the mutant preparation, we obtained direct evidence for a causal involvement of SK channels in the altered mAHP. In whole-cell recordings from CA1 pyramidal cells of B-raf$^{-/-}$ hippocampi, we found that the apamin-sensitive tail current after strong depolarization was markedly upregulated. Based on the

 doi:10.20944/preprints202506.2192.v1

functional profile of SK channels, it is well conceivable that the augmented SK current in B-raf-deficient neurons accounts for their reduced excitability, which manifested in our experiments as a decline in firing rate upon suprathreshold depolarization. This view receives support by our population spike (PS) recordings in the pyramidal cell body layer in which the SK channel blocker apamin produced a much stronger increase in PS amplitude in B-raf mutants than in controls.

In the distal dendrites and spines of hippocampal pyramidal cells, SK channels have been shown to be activated mainly by Ca^{2+} influx through NMDA receptors, which endows them with an immediate impact on the strength of NMDA-dependent synaptic plasticity [26]. Direct measurements of NMDA EPSCs in CA1 pyramidal cells voltage-clamped to +40 mV to record full-blown NMDA currents demonstrated a significant attenuation in the absence of B-raf signaling. Unlike the NMDA component, the AMPA-R-mediated component of excitatory synaptic transmission remained seemingly unaffected in the mutant preparation, as the routinely monitored field synaptic potentials to single stimuli leading mainly to AMPA-R activation did not differ between controls and B-raf mutants.

In contrast, a previous study on CA1 neurons in cultured hippocampal slices which were transfected with constitutively active or dominant-negative B-raf mutants using a rapid lentivirus-based gene replacement method, reported that loss-of-function and gain-of-function B-raf mutations produced a wide range of decreases and increases, respectively, in AMPA-R-mediated synaptic transmission, whereas NMDA currents remained unaffected [14]. Based on the results of a systematic replacement of the molecules that constitute the signaling cascade underlying LTP induction, the authors of that study arrived at the conclusion that B-raf serves as a universal signaling effector coupling NMDA-CamKII-SynGap-Ras signaling to the MEK-ERK pathway. In our hands, B-raf deficiency left AMPA responses largely intact, whereas the NMDA component of fPSPs that were evoked by a near-physiological triplet of stimuli [32] in the presence of an AMPA-R blocker exhibited an appreciable decrease in B-raf-deficient slices when compared to the wild type preparation.

Notably, the decline of the isolated NMDA component could be reversed by the SK channel blocker apamin. The augmenting effect of apamin on the NMDA component was much stronger in the mutant than in the wild type preparation, so that at the highest stimulation strength, the NMDA responses in the two genotypes converged onto the same maximal value making them virtually indistinguishable. This finding argues for a strong contribution of SK cannels to the dampened NMDA response.

Apart from general differences between cultured and acutely prepared brain slices as a source of inconsistent findings, the fact that the rapid gene replacement method of Lim et al. [14] appeared to have spared NMDA responses, suggests that the upregulation of SK current is a late consequence of B-raf deficiency. Thus, our study raises a number of intriguing questions to be followed up in future work. For example, does B-raf signaling directly target SK channels or is the enhanced SK current a rather slowly developing (mal)adaptive process? How is the increase in SK current achieved: are new channels produced and inserted in the cell membrane, or is the open probability of existing channels increased? Finally, would administration of a SK channel blocker reverse learning and memory deficits in B-raf-deficient mice and – in the long run – in patients suffering from loss-of-function B-raf mutations?

4. Materials and Methods

4.1. Animals

Adult (4-7 months old) male and female mice were used for experiments. B-raf knockout (B-raf$^{-/-}$) mice were obtained by breeding floxed B-raf (B-raf^{flox}) mice with transgenic CamkIIa-Cre mice [16, 17]. The littermates of homozygous B-raf^{flox} without Cre transgene were used as control. Such inactivation of the B-raf gene in forebrain principal neurons from two postnatal weeks impaired ERK/MAPK signaling activation [16, 17]. Mice were group-housed under standard conditions with light/dark cycle (7 am / 7 pm) and free access to water and food. All procedures were conducted in

 doi:10.20944/preprints202506.2192.v1

accordance with the Animal Protection Law of Germany and the European Communities Council Directive of November 1986 /86/609/EEC, and with approval of local government of Lower Franconia.

4.2. Electrophysiological Recordings from Brain Slices

Transversal brain slices (350 μm thick) containing the dorsal hippocampus were pre-pared from mice under isoflurane anesthesia. Brain slices were cut in ice-cold sucrose-based artificial cerebrospinal fluid (aCSF) containing (in mM) 75 sucrose, 87 NaCl, 3 KCl, 0.5 $CaCl_2$, 7 $MgCl_2$, 1.25 NaH_2PO_4, 25 $NaHCO_3$ and 10 D-glucose. Slices were incubated in same solution for 10 min at 35 °C and then in modified aCSF containing (in mM) 125 NaCl, 3 KCl, 1 $CaCl_2$, 3 $MgCl_2$, 1.25 NaH_2PO_4, 25 $NaHCO_3$ and 10 D-glucose at room temperature for at least 2 h before recording. Individual slices were then transferred to a submerged recording chamber perfused with standard aCSF with 1 mM $MgCl_2$ and 3 mM $CaCl_2$ (unless otherwise stated) at room temperature. All solutions were constantly gassed with 95% O_2 - 5% CO_2.

CA1 field postsynaptic potentials (fPSPs) and population spikes (PS) were recorded in the apical dendrites and the pyramidal cell layer, respectively, with a pipette filled with modified aCSF (in which $NaHCO_3$ was replaced by 5 mM HEPES to avoid pH change). A concentric bipolar electrode was inserted into the stratum radiatum to stimulate Schaffer collaterals (SC), with constant current pulses (0.1 ms width). Stimuli were delivered at different intensities, ranging from 60 μA to 200 μA or 400 μA, to construct input-output (I-O) curve of population responses. PS in the pyramidal cell bodies normally exhibit three peaks, and the amplitude was calculated as average of the negative peak from the two positive peaks around it. fPSP in the stratum radiatum has a negative peak, and the amplitude was measured as the value of peak negative from the preceding baseline. In some experiments, to maximize the NMDA component of fPSPs, CNQX (20 μM) was used to block AMPA receptor-mediated fPSPs, and burst pattern (3 stimuli at 100 Hz) was used to evoke NMDA receptor-mediated fPSPs. The effect of SK channel blocker apamin (125 nM) was tested with stimulus intensity set to induce 30-40% of maximal field potentials.

Whole-cell recordings were performed from visually identified CA1 pyramidal cells in the pyramidal cell layer, under voltage-clamp mode or current-clamp mode. For experiments to evaluate NMDA/AMPA ratio among excitatory synaptic transmission in voltage-clamped cells, the patch pipets were filled with (in mM) 130 CsCl, 2 $MgCl_2$, 2 Na_2ATP, 0.3 Na_3GTP, 5 QX-314, 5 HEPES, and 5 EGTA (pH 7.3). Excitatory postsynaptic current (EPSC) was evoked by stimulus via a bipolar electrode in stratum radium, in the presence of $GABA_A$ receptor antagonist picrotoxin (100 μM). The stimulus strength was set at the beginning of each experiment so that the EPSC peak was around 500 pA at a holding potential of -80 mV. The AMPA receptor-mediated EPSC (AMPA-EPSC) was isolated by subtracting EPSC in the presence of CNQX (20 μM) from that in its absence. The NMDA receptor mediated EPSC (NMDA-EPSC) was recorded at +40 mV in the presence of CNQX and subtracted from that in the presence of DL-APV (50 μM). Glycine (10 μM) was added into aCSF to ensure a saturating concentration of glycine for NMDA receptors.

To assess somatic SK channel activity and pyramidal cell excitability, the recording pipette contained (in mM) 135 K-gluconate, 4 NaCl, 10 KCl, 2 Na_2ATP, 0.3 Na_3GTP and 5 HEPES (pH 7.3), and the recordings were performed in aCSF with 2 mM $CaCl_2$ and 1 Mg $MgCl_2$. Tail currents in voltage-clamped pyramidal cells (Vh -60 mV) were evoked by a depolarizing command to +30 mV for 100 ms, thereby triggering sufficient calcium current to activate SK channels, in the presence of TTX (1 μM, to block sodium current) and tetraethylammonium (TEA, 5 mM; to block other potassium currents, e.g. voltage-dependent K^+ channel, large conductance calcium-activated potassium channels or BK channels). Recordings in the absence and presence of the selective SK channel blocker apamin (125 nM, added to inflowing bath solution) were used to isolate and quantify peak SK currents, which were determined *c.a.* 100 ms after stepping back to -60 mV). Further experiments to examine excitability of CA1 pyramidal cells were conducted in whole-cell current-clamp mode. To facilitate comparison between control and B-raf mutants, action potentials (APs) were evoked by depolarizing current pulses (50, 100 and 200 pA; 500 ms duration), with membrane potential set to -

 doi:10.20944/preprints202506.2192.v1

70 mV by current injection. AP properties were analyzed for the first AP in response to a 50 pA depolarizing step, including voltage threshold, rise time and amplitude of upstroke, and half-width. The medium afterhyperpolarization (mAHP), which partially involves SK channel activity (Storm, 1989; Bond et al., 2004), was measured 30-50 ms after repolarization.

All potentials were corrected for liquid junction potential (10 mV). Series resistance in the whole-cell voltage-clamp configuration was 10-20 MΩ and compensated by 60-80%. Signals were filtered at 2 kHz (for extracellular and whole-cell voltage-clamp recordings) and 6 kHz (for whole-cell current-clamp recordings) and sampled at 20 kHz using a Multiclamp 700B amplifier, in conjunction with Digidata 1440A interface and pClamp10.2 software (Molecular Devices, Sunnyvale, CA). MiniDigi 1A and AxoScope 10.2 were used for low-resolution scope recording, sampled at 1 kHz. Unless otherwise stated, drugs and chemicals were obtained from Tocris Bioscience (Bio-techne GmbH, Wiesbaden, Germany) and Sigma-Aldrich Chemie GmbH (Steinheim, Germany).

4.3. Statistical Analysis

Data analysis was performed off-line with Clampfit 10.2 (Molecular Devices, CA, USA). Data are expressed as means ± SEM. OriginPro 2018G (OriginLab Corporation, Northampton, MA, USA) was used for statistics and graphs. Shapiro-Wilk test was used to assess normality of data distribution, and the null hypothesis was accepted when p-value was larger than 0.05. Statistical comparisons were performed using unpaired or paired Student's t-test and one-way or two-way analysis of variance (ANOVA) followed by Tukey's post-hoc test, as appropriate. Significance was assumed for $p < 0.05$.

Author Contributions: C.R. and F.Z. performed recordings and analyzed data. F.Z. designed the experiments and wrote the paper. C.A. supervised the project and revised the manuscript.

Funding: This study was support by intramural funds.

Institutional Review Board Statement: The study was conducted in accordance with German and international guidelines and regulations of the care and treatment of laboratory animals of the European Communities Council Directive of 24 November 1986 (86/609/EEC).

Data Availability Statement: Data of this study are available from the corresponding author upon reasonable request.

Acknowledgments: We thank Maria Schulte, Iwona Izydorczyk and Birgit Vogler for technical help. We thank Dr. Benedikt Wefers and Dr. Ralf Kühn (Institute of Developmental Genetics, Helmholtz Zentrum München, Germany) for B-raf transgenic mice.

Conflicts of Interest: The authors declare no conflicts of interest.

Abbreviations

The following abbreviations are used in this manuscript: aCSF, artificial cerebrospinal fluid; AP, action potential; AMPA-R, AMPA receptor; B-raf, type B isoform of rapidly accelerated fibrosarcom; ERK/MARK, extracellular signal-regulated kinase/mitogen-activated protein kinase; I-O, input-output curve; LTP, long-term potentiation; EPSC, excitatory postsynaptic current; fPSP, field postsynaptic potential; mAHP, medium afterhyperpolarization; NMDA-R, NMDA receptor; PS, population spike; SC, Schaffer collaterals; SK, small-conductance Ca^{2+}-activated K^+ channels; TEA, tetraethylammonium; TTX, tetrodotoxin.

References

1. Adams, J.P.; Sweatt, J.D. Molecular psychology: roles for the ERK MAP kinase cascade in memory. *Annu Rev Pharmacol Toxicol* **2002**, 42, 135-163. DOI: 10.1146/annurev.pharmtox.42.082701.145401
2. Wellbrock, C.; Karasarides, M.; Marais, R. The RAF proteins take centre stage. *Nat Rev Mol Cell Biol* **2004**, 5, 875-885. DOI: 10.1038/nrm1498

 doi:10.20944/preprints202506.2192.v1

3. Valluet, A.; Hmitou, I.; Davis, S.; Druillennec, S.; Larcher, M.; Laroche, S.; Eychène, A. B-raf alternative splicing is dispensable for development but required for learning and memory associated with the hippocampus in the adult mouse. *PLoS One* **2010**, 5, e15272. doi: 10.1371/journal.pone
4. Matallanas, D.; Birtwistle, M.; Romano, D.; Zebisch, A.; Rauch, J.; von Kriegsheim, A.; Kolch, W. Raf family kinases: old dogs have learned new tricks. *Genes Cancer* **2011**, 2, 232-260. doi: 10.1177/1947601911407323
5. Pfeiffer, V.; Götz, R.; Xiang, C.; Camarero, G.; Braun, A.; Zhang, Y.; Blum, R.; Heinsen, H.; Nieswandt, B.; Rapp, U.R. Ablation of BRaf impairs neuronal differentiation in the postnatal hippocampus and cerebellum. *PLoS One* **2013**, 8, e58259. doi: 10.1371/journal.pone.0058259
6. Papin, C.; Eychène, A.; Brunet, A.; Pagès, G.; Pouysségur, J.; Calothy, G.; Barnier, J.V. B-Raf protein isoforms interact with and phosphorylate Mek-1 on serine residues 218 and 222. *Oncogene* **1995**,10, 1647-1651.
7. Marais, R.; Light, Y.; Paterson, H.F.; Mason, C.S.; Marshall, C.J. Differential regulation of Raf-1, A-Raf, and B-Raf by oncogenic ras and tyrosine kinases. *J Biol Chem*. **1997**, 272, 4378-4383. doi: 10.1074/jbc.272.7.4378
8. Roberts, P.J.; Der, C.J. Targeting the Raf-MEK-ERK mitogen-activated protein kinase cascade for the treatment of cancer. *Oncogene* **2007**, 26, 3291-3310. doi: 10.1038/sj.onc.1210422
9. Karoulia. Z.; Gavathiotis, E.; Poulikakos, P.I. New perspectives for targeting RAF kinase in human cancer. *Nat Rev Cancer* **2017**, 17, 676-691. doi: 10.1038/nrc.2017.79
10. Maraka, S.; Janku, F. BRAF alterations in primary brain tumors. *Discov Med*. **2018**, 26, 51-60.
11. Anaya, Y.A.; Bracho, R.P.; Chauhan, S.C.; Tripathi, M.K.; Bandyopadhyay, D. Small molecule B-RAF inhibitors as anti-cancer therapeutics: advances in discovery, development, and mechanistic insights. *Int J Mol Sci.* **2025**, 26, 2676. doi: 10.3390/ijms26062676
12. Barnier, J.V.; Papin, C.; Eychène, A.; Lecoq, O.; Calothy, G. The mouse B-raf gene encodes multiple protein isoforms with tissue-specific expression. *J Biol Chem*. **1995**, 270, 23381-23389. doi: 10.1074/jbc.270.40.23381
13. Morice, C.; Nothias, F.; König, S.; Vernier, P.; Baccarini, M.; Vincent, J.D.; Barnier, J.V. Raf-1 and B-Raf proteins have similar regional distributions but differential subcellular localization in adult rat brain. *Eur J Neurosci*. **1999**, 11, 1995-2006. doi: 10.1046/j.1460-9568.1999.00609.x
14. Lim, C.S.; Kang, X.; Mirabella, V.; Zhang, H.; Bu, Q.; Araki, Y.; Hoang, E.T.; Wang, S.; Shen, Y.; Choi, S.; Kaang, B.K.; Chang, Q.; Pang, Z.P.; Huganir, R.L; Zhu, J.J. B-Raf signaling principles unveiled by large-scale human mutation analysis with a rapid lentivirus-based gene replacement method. *Genes Dev*. **2017**, 31, 537-552. doi: 10.1101/gad.294413.116
15. Wojnowski, L.; Zimmer, A.M.; Beck, T.W.; Hahn, H.; Bernal, R.; Rapp, U.R.; Zimmer, A. Endothelial apoptosis in Braf-deficient mice. *Nat Genet* **1997**, 16, 293-297. DOI: 10.1038/ng0797-293
16. Chen, A.P.; Ohno, M.; Giese, K.P.; Kühn, R.; Chen, R.L.; Silva, A.J. Forebrain-specific knockout of B-raf kinase leads to deficits in hippocampal long-term potentiation, learning, and memory. *J Neurosci Res*. **2006**, 83, 28-38. doi: 10.1002/jnr.20703
17. Wefers, B.; Hitz, C.; Hölter, S.M.; Trümbach, D.; Hansen, J.; Weber, P.; Pütz, B.; Deussing, J.M.; de Angelis, M.H., Roenneberg, T.; Zheng, F.; Alzheimer, C.; Silva, A.; Wurst, W.; Kühn, R. MAPK signaling determines anxiety in the juvenile mouse brain but depression-like behavior in adults. *PLoS One* **2012**, 7, e35035. doi: 10.1371/journal.pone.0035035
18. Malenka, R.C.; Bear, M.F. LTP and LTD: an embarrassment of riches. *Neuron* **2004**, 44, 5-21. doi: 10.1016/j.neuron.2004.09.012.
19. Lüscher, C.; Malenka, R.C. NMDA receptor-dependent long-term potentiation and long-term depression (LTP/LTD). *Cold Spring Harb Perspect Biol*. **2012**, 4, a005710. doi: 10.1101/cshperspect.a005710
20. Xia, X.M.; Fakler, B.; Rivard, A.; Wayman, G.; Johnson-Pais, T.; Keen, J.E.; Ishii, T.; Hirschberg, B.; Bond, C.T.; Lutsenko, S.; Maylie, J.; Adelman, J.P. Mechanism of calcium gating in small-conductance calcium-activated potassium channels. *Nature* **1998**, 395, 503-507. doi: 10.1038/26758
21. Tzounopoulos, T.; Stackman, R. Enhancing synaptic plasticity and memory: a role for small-conductance Ca^{2+}-activated K^+ channels. *Neuroscientist* **2003**, 9, 434-439. doi: 10.1177/1073858403259282
22. Bond, C.T.; Maylie, J.; Adelman, J.P. SK channels in excitability, pacemaking and synaptic integration. *Curr Opin Neurobiol*. **2005**, 15, 305-311. doi: 10.1016/j.conb.2005.05.001
23. Adelman, J.P.; Maylie, J.; Sah, P. Small-conductance Ca^{2+}-activated K^+ channels: form and function. *Annu Rev Physiol*. **2012**, 74, 245-269. doi: 10.1146/annurev-physiol-020911-153336

 doi:10.20944/preprints202506.2192.v1

24. Stocker, M.; Pedarzani, P. Differential distribution of three Ca^{2+}-activated K^+ channel subunits, SK1, SK2, and SK3, in the adult rat central nervous system. *Mol Cell Neurosci.* **2000**, 15, 476-493. doi: 10.1006/mcne.2000.0842
25. Sailer, C.A.; Kaufmann, W.A.; Marksteiner, J.; Knaus, H.G. Comparative immunohistochemical distribution of three small-conductance Ca^{2+}-activated potassium channel subunits, SK1, SK2, and SK3 in mouse brain. *Mol Cell Neurosci*. **2004**, 26, 458-469. doi: 10.1016/j.mcn.2004.03.002
26. Ngo-Anh, T.J.; Bloodgood, B.L.; Lin, M.; Sabatini, B.L.; Maylie, J.; Adelman, J.P. SK channels and NMDA receptors form a Ca^{2+}-mediated feedback loop in dendritic spines. *Nat Neurosci*. **2005**, 8, 642-649. doi: 10.1038/nn1449
27. Faber, E.S.; Delaney, A.J.; Sah, P. SK channels regulate excitatory synaptic transmission and plasticity in the lateral amygdala. *Nat Neurosci.* **2005**, 8, 635-641. doi: 10.1038/nn1450
28. Faber, ES. Functional interplay between NMDA receptors, SK channels and voltage-gated Ca^{2+} channels regulate synaptic excitability in the medial prefrontal cortex. *J Physiol*. **2010**, 588, 1281-1292. doi: 10.1113/jphysiol.2009.185645
29. Behnisch, T.; Reymann, K.G. Inhibition of apamin-sensitive calcium dependent potassium channels facilitate the induction of long-term potentiation in the CA1 region of rat hippocampus in vitro. *Neurosci Lett* **1998**, 253, 91-94. DOI: 10.1016/s0304-3940(98)00612-0
30. Lin, M.T.; Lujan, R.; Watanabe, M.; Frerking, M.; Maylie, J.; Adelman, J.P. Coupled activity-dependent trafficking of synaptic SK2 channels and AMPA receptors. *J Neurosci* **2010**, 30, 11726-11734. DOI: 10.1523/JNEUROSCI.1411-10.2010
31. Hammond, R.S.; Bond, C.T.; Strassmaier, T.; Ngo-Anh, T.J.; Adelman, J.P.; Maylie, J.; Stackman, R.W. Small-conductance Ca^{2+}-activated K^+ channel type 2 (SK2) modulates hippocampal learning, memory, and synaptic plasticity. *J Neurosci* **2006**, 26, 1844-1853. DOI: 10.1523/JNEUROSCI.4106-05.2006
32. Ranck, J.B. Jr. Studies on single neurons in dorsal hippocampal formation and septum in unrestrained rats. I. Behavioral correlates and firing repertoires. *Exp Neurol.* **1973**, 41, 461-531.
33. Stocker, M. Ca^{2+}-activated K^+ channels: molecular determinants and function of the SK family. *Nat Rev Neurosci.* **2004,** 5, 758-770. doi: 10.1038/nrn1516
34. Tonini, R.; Ferraro, T.; Sampedro-Castañeda, M.; Cavaccini, A.; Stocker, M.; Richards, C.D.; Pedarzani, P. Small-conductance Ca^{2+}-activated K^+ channels modulate action potential-induced Ca^{2+} transients in hippocampal neurons. *J Neurophysiol*. **2013**, 109, 1514-1524. doi: 10.1152/jn.00346.2012
35. Storm, J.F. An afterhyperpolarization of medium duration in rat hippocampal pyramidal cells. *J Physiol. (Lond.)* **1989**, 409, 171-190. DOI: 10.1113/jphysiol.1989.sp017491
36. Bond, C.T.; Herson, P.S.; Strassmaier, T.; Hammond, R.; Stackman, R.; Maylie, J.; Adelman, J.P. Small conductance Ca^{2+}-activated K^+ channel knockout mice reveal the identity of calcium-dependent afterhyperpolarization currents. *J Neurosci.* **2004**, 24, 5301-5306. doi: 10.1523/JNEUROSCI.0182-04.2004
37. Stocker, M.; Hirzel, K.; D'hoedt, D.; Pedarzani, P. Matching molecules to function: neuronal Ca^{2+}-activated K^+ channels and afterhyperpolarizations. *Toxicon* **2004**, 43, 933-949. doi: 10.1016/j.toxicon.2003.12.009
38. Pedarzani, P.; McCutcheon, J.E.; Rogge, G.; Jensen, B.S., Christophersen, P.; Hougaard, C.; Strøbaek, D.; Stocker, M. Specific enhancement of SK channel activity selectively potentiates the afterhyperpolarizing current I(AHP) and modulates the firing properties of hippocampal pyramidal neurons. *J Biol Chem*. **2005**, 280, 41404-41411. doi: 10.1074/jbc.M509610200